Geophysical Journal International

Geophys. J. Int. (2011) **184,** 860–868 doi: 10.1111/j.1365-246X.2010.04886.x

Seasonal variations of observed noise amplitudes at 2–18 Hz in southern California

G. Hillers[1]* and Y. Ben-Zion[2]

[1]*Seismological Laboratory, California Institute of Technology Pasadena, California, USA. E-mail: gregor@gps.caltech.edu*
[2]*Department of Earth Sciences, University of Southern California Los Angeles, California, USA*

Accepted 2010 November 9. Received 2010 September 20; in original form 2010 May 20

SUMMARY

We show that noise amplitudes at frequencies above 1 Hz exhibit strong seasonal variations in a broad southern California region. The results are based on 3-component seismic data recorded between 2002 and 2009 by 30 stations. Focusing on continuous 6-hr night-time segments, the seismograms are bandpass-filtered in nine frequency bands between 2 and 18 Hz. Squared amplitudes are median-filtered to reduce the influence of earthquake signals and integrated to yield half-hourly noise energy estimates. The 6-hr minimum energy values are converted back to ground velocity and used as representative daily noise level amplitudes. Notwithstanding various trends, drifts and other transient complexities, a common feature of the resulting time series in both the horizontal and vertical components are annual amplitude changes at all examined frequencies and all stations. The strength of amplitude variations shows no correlation with distance from the coast and some particularly clear seasonal changes are seen near topographic features in arid uninhabited areas. Comparison to meteorological data suggests that the main sources for the high-frequency noise field are variations of temperature and wind at the surface. In addition to acting directly on topographic irregularities and other surface features, these sources (and especially temperature changes) may also generate high-frequency noise by inducing multitudinous small-scale failures in the shallow crust.

Key words: Geomechanics; Elasticity and anelasticity; Fracture and flow; Site effects; Wave scattering and diffraction; Wave propagation.

1 INTRODUCTION

Ambient seismic noise refers to ground motions recorded continuously by seismographs in the absence of earthquakes, explosions and other large impulsive sources. Knowledge of the spatial and temporal variations of the ambient noise at different frequencies is essential for assessing the detection capability of individual seismic stations and networks. Understanding the various sources that generate the noise as functions of space, time and frequency can provide important information on continual natural processes and the response of various Earth sections to the operating sources.

Synthesised noise curves based on stacking of many records in regional and global data sets follow a general frequency-dependent pattern of (minimum) noise amplitudes, with systematic level differences between horizontal and vertical components (Peterson 1993; Berger *et al.* 2004; McNamara & Buland 2004). The main common features of noise models based on the analyses done to date include long period noise, Earth's free oscillations, microseisms and high frequency noise.

Noise at long periods above 500 s is usually attributed to long wavelength ground tilting caused by temperature fluctuations or large scale atmospheric pressure changes (e.g. Beauduin *et al.* 1996), which are correlated with seasonal climatic changes and result in larger noise amplitudes on horizontal components. The range between periods of 40 s and 550 s, where lowest noise amplitudes are observed, includes a small peak around 100 s consisting of a series of distinct monochromatic oscillations, referred to as Earth's 'hum' (Rhie & Romanowicz 2004; Tanimoto 2005; Kurrle & Widmer-Schnidrig 2008). While the source of sustained toroidal oscillations is less understood, long period Rayleigh waves associated with spheroidal modes are continuously generated by atmosphere–ocean–seafloor interactions (Webb 2007), leading to a 6-month periodicity in the generated amplitudes due to semi-hemispheric ocean-wave activities (Rhie & Romanowicz 2004).

At 14 s and 7 s the noise amplitude spectrum is dominated by the primary and secondary microseisms peaks, respectively, associated primarily with Rayleigh waves generated by ocean wave–seafloor

*Now at: LGIT-Grenoble, Université Joseph Fourier Saint Martin d'Heres, France.

interactions (Longuet-Higgins 1950). In contrast to hum excitation, the mechanism responsible for the larger double frequency peak requires roughly opposite travelling waves that are either generated by coastal reflections (Tanimoto *et al.* 2006), or opposing wind pattern over specific bathymetric locations (Kedar *et al.* 2008). Seasonal amplitude changes of the microseisms peaks follow the global weather pattern and exhibit decaying signal strength away from coastlines. Similarly, specific conditions off the west African coast result in a globally observable yet smaller microseism peak at 26 s (e.g. Shapiro *et al.* 2006, and references therein).

Analysis of noise around 1 Hz tends to focus on surface Rayleigh waves generated under conditions similar to microseisms, that is, by water body-solid Earth interactions, but contain also body waves that sample deeper parts of Earth (Koper & de Foy 2008; Koper *et al.* 2009; Zhan *et al.* 2010). Energies at frequencies above 1 Hz are usually attributed to cultural noise, which propagates mainly as rapidly-attenuating high-frequency surface waves, manifested by significantly reduced noise amplitudes in boreholes (Gurrola *et al.* 1990), tunnels, and mines. Diurnal and weekly variations of cultural noise (Ringdal & Bungum 1977) affect earthquake detection capabilities (Atef *et al.* 2009). Wind acting on topographic irregularities or trees and posts can also transmit energy into the ground at high frequencies and the associated ground tilting may produce longer period noise. Temporal variations associated with changing weather patterns, as well as spring run-offs and changes in snow covers in mountainous or cold-climate areas, can cause seasonal noise level changes at high frequencies. While Ringdal & Bungum (1977) observed seasonal changes in noise amplitudes between 1.2 Hz and 3.2 Hz using three years of data from NORSAR array, Norway, systematic seasonal changes in noise amplitudes at higher frequencies covering a large area were studied less extensively.

In the present paper, we analyse noise amplitudes at frequencies between 2 and 18 Hz, using seven years of continuous seismic data recorded at 30 stations between 239 and 245 degree longitude and 33–35.5 degree latitude in southern California. The analysis reveals seasonal changes at all examined stations, components of motion and frequency bands. Significantly, the amplitude variations show no correlation with distance from the coast and some strong seasonal variations are observed near topographic features in desert areas. The large area coverage, spatial pattern of observed amplitudes, existence of signals in both horizontal and vertical components, strong signals in uninhabited arid regions and correlation with collocated wind speed and temperature measurements imply that the signals are unlikely to originate from ocean waves, variations of ground water levels or surface water flow. The observed high-frequency noise signals are likely dominated by local atmospheric sources associated with wind and temperature variations. These sources can produce noise by direct loading of surface features, as well as by inducing continual occurrence of small-scale failures in the shallow crust. In particular, the interaction of atmospheric temperature changes with large-scale variations of topography, lithology and other surface properties can produce thermoelastic strain with appreciable amplitude and related local brittle failures over a depth section of several kilometres.

2 DATA ANALYSIS

We analyse continuous three component seismograms recorded at 30 broadband stations in southern California (Fig. 1) between 2002 and 2009. We restrict the analysis to 6-hr night-time segments to reduce the influence of cultural activity. The following procedure describes our processing steps to estimate a representative minimum daily noise amplitude value for horizontal and vertical components.

Data are retrieved from the Southern California Earthquake Data Center, where amplitude counts are converted to ground velocity using a constant, station specific conversion factor. The 20 or 40 Hz sampled seismograms (Fig. 2a) are bandpass filtered in 2 Hz intervals between 2 and 18 Hz (Fig. 2b), with 2 Hz-data filtered between

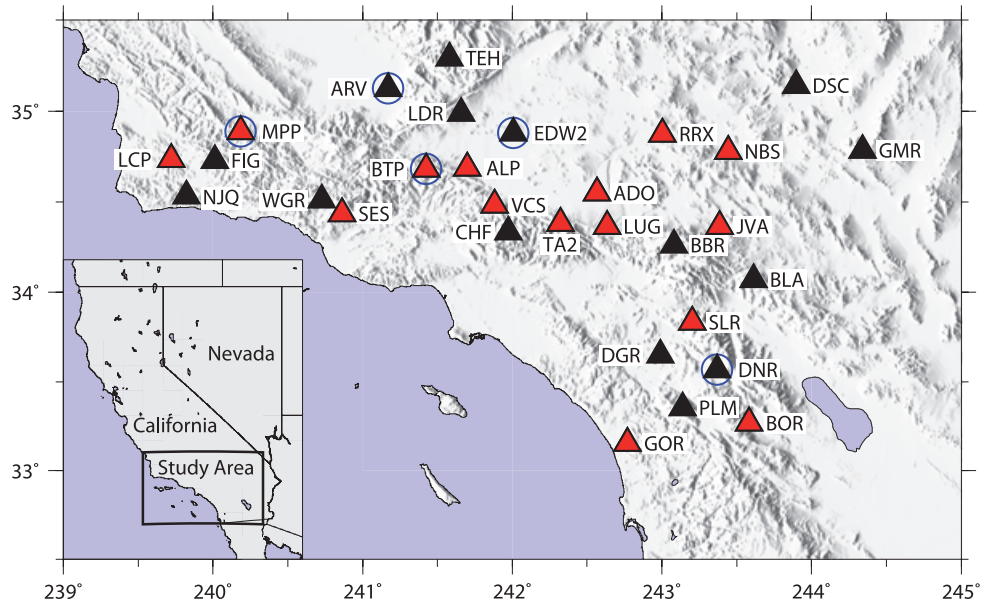

Figure 1. Locations of 30 broadband stations from the Southern California Seismic Network (SCSN) used to analyse seven years of continuous 3-component seismic data for noise amplitudes in nine frequency bands between 2 and 18 Hz. The stations cover a substantial area and many are situated in uninhabited arid regions, with small expected effects from cultural activities and water flow on noise amplitudes in the considered frequency range. Fig. 3 gives example analysis results from data of the stations indicated in blue and corresponding results from the other stations are provided in the supplementary material. Data from stations in red show the largest seasonal amplitude variations. Additional information on the spatial distribution of amplitudes is presented in Figs. 4 and S2.

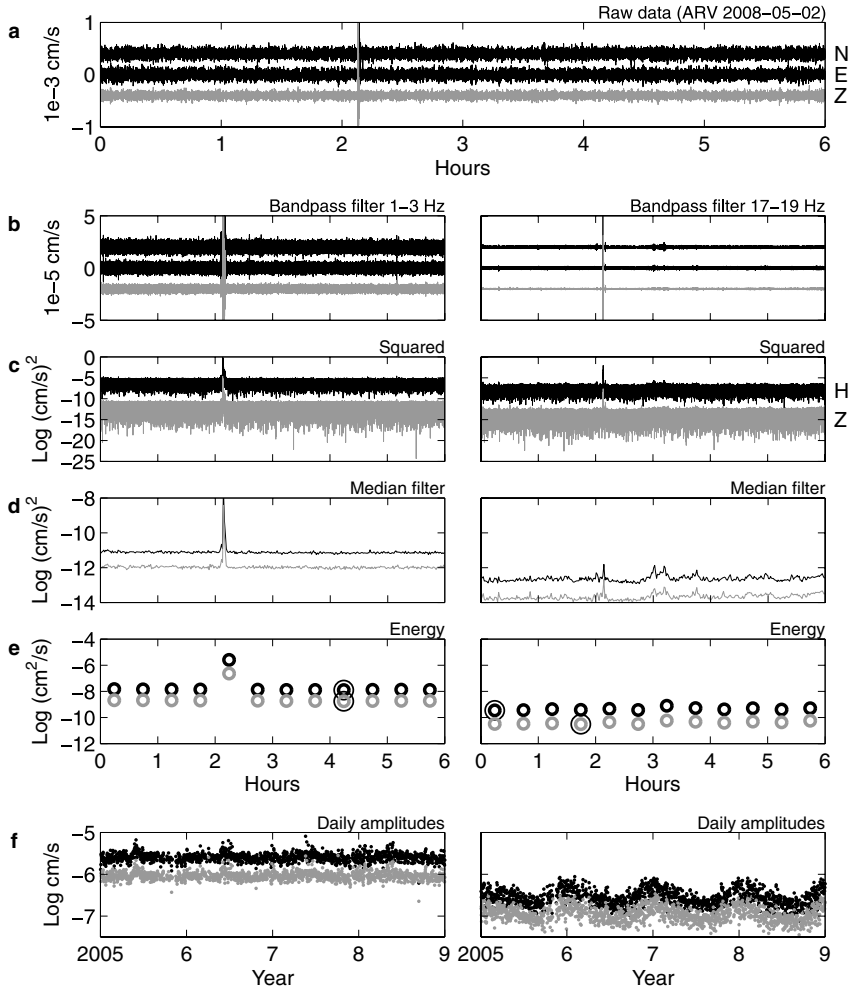

Figure 2. Illustration of the processing steps to estimate representative daily noise amplitude values from continuous 3-component seismograms. (a) Continuous data recorded during six night-time hours sampled at 20 Hz or 40 Hz. Black and grey data correspond to horizontal and vertical components, respectively. Data are on the same scale, offset for enhanced visibility. A M3.5 earthquake occurred in 15 km distance from station ARV (visible between 2–3 hr). (b) Bandpass filtered data between 1–3 Hz (left, referred to as 2 Hz filtered) and 17–19 Hz (right, referred to as 18 Hz filtered). Data are on the same scale, offset. After filtering, components N and E are merged to one horizontal component, $H = \sqrt{N^2 + E^2}$. (c) Squared amplitudes of the horizontal and the vertical components, respectively. Data are on the same scale, offset. (d) Application of a median filter. Data are on the same scale and not offset. Note the difference in noise amplitudes between H and V (equivalent to Z) components and the difference in earthquake amplitudes between the two frequency bands. (e) Estimation of energies in non-overlapping 30 min intervals. Data are on the same scale and not offset. The minimum energy values of H (black circles) and V (grey circles) data during the six hours are chosen and transferred back to velocity to obtain representative amplitude values. (f) Daily sampled time series of noise amplitude measurements of the H and V components between 2005 and 2009. Data are on the same scale and not offset. Note the pronounced seasonal variations in the high frequency band. Significantly lower amplitude levels compared to the 2 Hz data are mainly due to effects of the anti-alias filter (Fig. S3).

1 and 3 Hz, 4 Hz-data between 3 and 5 Hz, etc. We compute the root-mean-square value of the north (N) and east (E) amplitudes and use it as the averaged horizontal (H) component. Toward obtaining estimates of seismic energy, we square the values of the horizontal and vertical component amplitudes (Fig. 2c). To reduce the influence of large amplitude signals such as earthquakes on energy estimates, the data are median filtered and down sampled (Fig. 2d) by selecting the median amplitude value in subsequent 30 s windows around the centre sample. The resulting time series are then integrated to yield energy measurements for non-overlapping 30 min time windows (Fig. 2e). Finally, to obtain time series of daily sampled low noise amplitude estimates (Fig. 2f), the respective 6-hr minimum energy values of horizontal and vertical components are converted back to velocity.

Amplitude spectral power densities are computed (Figs 3 and S1) using a Lomb-Scargle algorithm to account for irregular sampling due to problems with station performance or maintenance. Small sidelobes in the spectral power estimates at multiples of the 1 per year peak are insignificant, except for a small number of frequency bands at individual stations (e.g. 2 per year periodicity at low frequencies at ARV, BTP). To visually enhance trends for individual time series, outliers are removed and time series are smoothed with a running 60 day average filter (Tanimoto *et al.* 2006). The median amplitudes of the smoothed time series represent the average station and frequency dependent noise levels (Fig. 4) and maximum annual changes (Fig. S2) are found by measuring the difference between the maximum and minimum amplitude values in each calendar year.

Estimates of daily noise levels in the 8 and 18 Hz bands, that is, filtered between 7 and 9 Hz and 17 and 19 Hz, respectively, are biased somewhat by the high frequency amplitude reduction resulting from the anti-alias filter of the 20 and 40 Hz sampled data

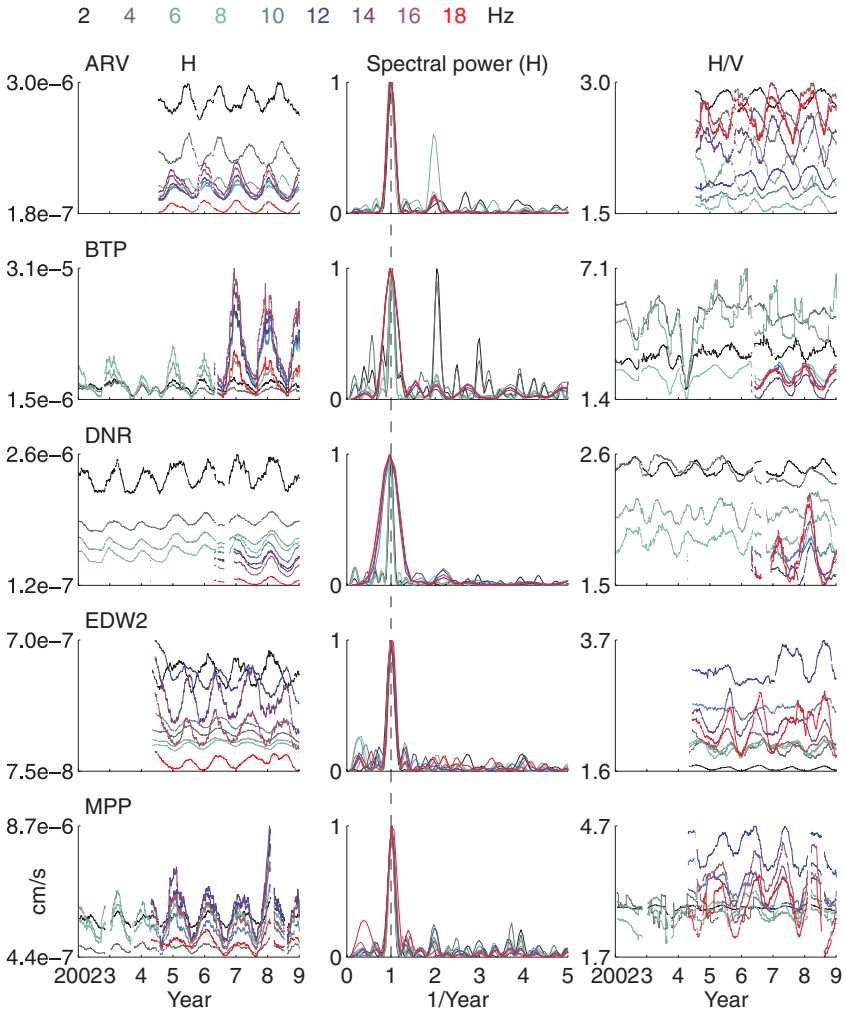

Figure 3. Results of noise amplitude measurements at stations (names on top left) indicated in blue in Fig. 1 (corresponding results from all stations are shown in Fig. S1). This subset was chosen because it exhibits a clean seasonal signal observable on the H (and V, not shown) components. Left: smoothed horizontal noise amplitude time series at nine frequency bands (colours correspond to the frequency values on top), derived from daily noise level measurements (Fig. 2f). The y-axis is linear and clipped at the overall minimum and maximum values measured at each station. Note the scale differences among the five stations. Centre: power spectral densities derived from the original irregularly sampled noise level time series (Fig. 2f). Each spectrum is scaled to the maximum value between 0.5 per year and 1.5 per year. The y-axis is linear and clipped at 1. Right: ratio of horizontal (left) to vertical noise amplitudes at different frequency bands.

(Fig. S3). For the 8 Hz band the peak in 2004 at ADO (Fig. S1) results from an intermittent change to 40 Hz sampling. Similarly, at some stations small offsets in the 8 Hz data can be observed when the sampling rate was constantly changed from 20 to 40 Hz. We do not explicitly correct the data for these steps, which may introduce artefacts in the corresponding spectral power estimates, but we exclude the affected years from the analysis of maximum amplitude changes. Amplitudes for the 18 Hz band are potentially systematically underestimated, but the main results of the spectral analysis remain unaffected. Few other step-like amplitude changes (BLA, CHF, GOR, SES, Fig. S1) could be attributed to variable station operation parameters; the results and conclusions of our analysis are not affected by these irregularities and hence we do not correct for them.

We investigate possible source mechanisms of the observed noise amplitude changes by analysing hourly sampled wind speed and atmospheric temperature data recorded in the vicinity of seismic stations that show large noise amplitude changes (available at the California Data Exchange Center of the Department of Water Resources, http://cdec.water.ca.gov/). The loading associated with thermoelastic strain requires the atmospheric temperature field to propagate below ∼1 m unconsolidated surface layer (Ben-Zion & Leary 1986), leading to a phase delay between temperature and noise time series. In contrast, seismic noise generation associated with wind should propagate with essentially no delay. Therefore, the employed temperature data are based on daily averages of observed values, while the wind speed data are associated with averages computed for the same night-time periods used for the noise amplitude estimate.

3 RESULTS

The resulting seismic noise time series contain (as expected) a variety of complex signals including long term trends, drifts, occasional rapid changes and apparent erratic behaviour. These complexities notwithstanding, a general feature of the results is the existence of systematic seasonal amplitude changes, observable at all examined

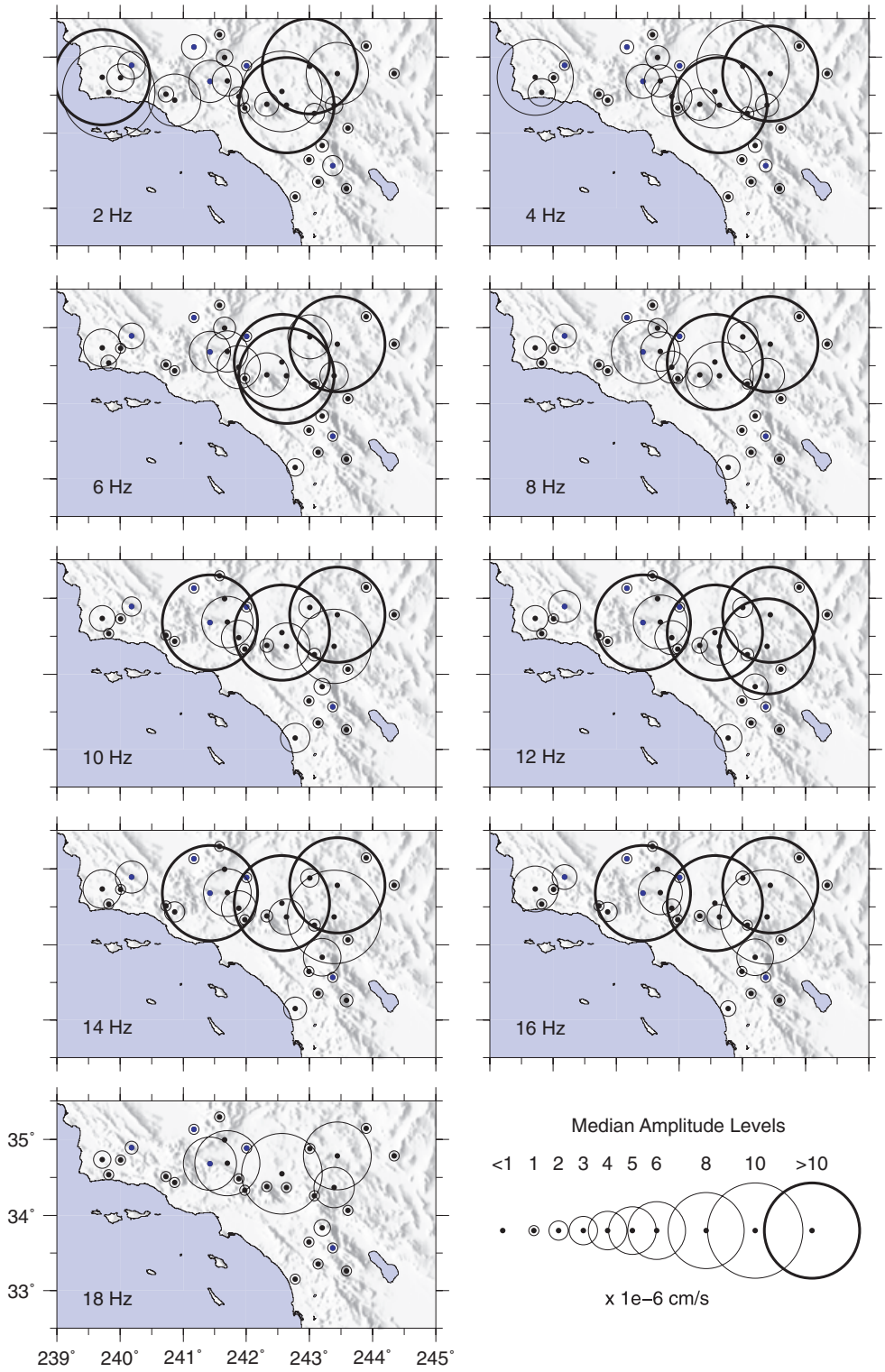

Figure 4. Spatial distribution of median H noise amplitude levels derived from time series in Figure S1, left. For all nine frequency bands (values in lower left of each frame), the amplitude levels are largest at stations especially near strong topographic gradients. Blue dots correspond to stations indicated in Fig. 1 and used in Fig. 3.

instruments, components of motion and frequencies. There are clear persisting differences in the strength of the amplitude variations at different stations, discussed below, along with occasional changes of phases and amplitudes at individual stations, for different frequencies, at horizontal and/or vertical channels.

The spatial pattern of median horizontal amplitudes (Fig. 4) shows a concentration of relatively high noise levels at stations located in and near the perimeter of the Mojave desert for all examined frequency bands. Stations in the north-west have increased amplitudes at 2 and 4 Hz, which may be influenced to some extent

by large microseisms amplitudes. Similarly, the pattern of noise amplitude variations (i.e. differences between maximum and minimum annual values) also has a concentration of large values at stations in and around the Mojave desert (Fig. S2). The most significant amplitude changes are observed at stations located near strong topographic variations (see also red triangles in Fig. 1). The data show no correlation of amplitude changes with distance from the coastline, so oceanic sources are unlikely to govern the observed seasonal variations, and comparison to wind speed and temperature data (Section 5) suggest that most variations are dominated by changes in local meteorological quantities. In addition to the ubiquitous seasonal changes at all stations, which are the focus of the present work, we highlight curious features observed at individual stations or a subset of stations using the following notations: H - horizontal amplitude, S - spectral power, H/V - horizontal to vertical amplitude ratio (see Figs. 3 and S1).

H. Phase shifts of half a year between time series filtered at lower and higher frequencies are observable at stations ARV, DSC, EDW2, GOR.

H. Amplitude changes do not scale linearly with bandpass filter frequency. While at BTP higher frequencies show consistently larger amplitude changes and average noise levels compared to lower frequencies (at 2–16 Hz), results at CHF, DNR, GMR and RRX show an inverse behaviour. In contrast, patterns at ADO, ARV, BBR, EDW2, GOR, LCP, MPP, NBS and VCS are more complex, exhibiting decreasing and increasing amplitude changes and average noise levels.

S. While most power in the 7-year time series is usually contained at 1 per year, time series at stations ARV, BTP, LCP show also significant power at 2 per year, at variable frequency bands.

H/V. Except for some frequencies at stations BLA, DSC, LDR, LUG, TA2 and TEH, horizontal amplitudes are consistently larger compared to vertical amplitudes, mostly by a factor 1–4.

H, H/V. The order of amplitude levels as a function of frequency observed on the horizontal channels is not preserved at the H/V levels.

H, H/V. Time series of H and H/V amplitudes can be either in phase (ARV, BLA, JVA, MPP) or out of phase (ALP, BBR, BOR, DGR, DNR, DSC, LDR).

H, H/V. Amplitudes on the horizontal channel of stations BTP, RRX are in phase for all frequencies, while the H/V amplitudes show phase shifts among different frequency bands.

H, H/V. Amplitudes on the horizontal channel of EDW2 are not in phase among all frequencies and the corresponding H/V amplitude time series do (2 Hz) and do not (14 Hz) show phase shifts with respect to the H time series, respectively.

Further analysis of some of these signals will be the subject of future work.

4 DISCUSSION AND CONCLUSIONS

Several studies provided evidence for high frequency noise in seismic data that can be associated with a variety of possible source mechanisms, such as cultural activities, local wind speeds and atmospheric disturbances coupled to solid Earth through oceanic processes (Young *et al.* 1994; Koper & de Foy 2008; Koper *et al.* 2009; Zhang *et al.* 2009; Zhan *et al.* 2010). High frequency noise may also be produced by processes related to recent observations done in the context of earthquake studies. Fischer *et al.* (2008a,b) observed bursts of high frequency waves in the shallow crust during the passage of seismic waves from nearby earthquakes. The removal of long period amplitude fluctuations in time series analysed with tectonic tremor detection methods (Brudzinski & Allen 2007; Nadeau & Guilhem 2009) also suggests significant amplitude changes at frequencies around 5 Hz.

Our analysis of continuous 3-component seismic data at 30 broadband stations in southern California documents the widespread existence of annual variations of noise amplitudes over the frequency range 2–18 Hz. Explaining the observed results requires a mechanism for ongoing generation of high frequency waves, along with a seasonal loading mechanism that is consistent with the observed spatial pattern of amplitudes. Two likely source mechanisms for the observations documented in Figs 3 and 4 (and S1, S2) are local atmospheric forces associated with wind and temperature fields. To examine the plausibility of these mechanisms, we compare time series of seismic noise amplitudes to available wind speed and air temperature data recorded in the vicinity of sites that show strong annual seismic noise changes.

We find that site specific noise amplitudes correlate with temperature changes (Figs 5a and b), variations in wind speed (Figs 5c and d) or a combination of both and occasionally with some other not yet determined mechanism. Variations in high frequency noise recorded at station BOR (Fig. 5a) correlate best with the local temperature curves peaking in summer and the observed lag between temperature and noise amplitude peaks are compatible with the thermoelastic strain mechanism (Ben-Zion & Leary 1986). Wind speed peaks in winter and hence local wind pattern and offshore sources are unlikely to dominate the high frequency noise at this site. Noise amplitudes at station TA2 (Fig. 5b) show a similar phase delay with respect to temperature, but the increase in noise levels also coincide with increases in overall low wind speeds. Here, a mixture of source processes may be responsible for the seismic noise at this site. Stations BTP and ALP (Figs 5c and d) provide examples of noise characteristics that may be controlled mainly by local wind pattern, since the noise does not lag behind the temperature. We note that anti-correlation of the type seen in BTP may simply reflect the lateral position of the station within the spatial temperature field. Interestingly, wind speed behaviour recorded in the vicinity of both stations is phase-shifted by about half a year, although the interstation distance is only a few kilometres, while the temperature profiles are in phase. This highlights the sensitivity of high-frequency noise fields to very local source processes. In general, we find that temperature variations are smooth across the focus area, but wind speeds are more erratic and can differ significantly over short spatial scales and even between day and night averages at individual sensors. Results at most other stations considered show no clear (anti-)correlation to a specific measurement, similar to TA2 and suggest that the local seismic noise fields originate by a variety of processes, which may become dominant at different times. Analysis of surface and borehole seismic data may provide stronger constraints on the source mechanisms that are dominant in different circumstances. However, this is beyond the scope of the present work.

Wind speed affects noise amplitudes by loading surface features, predominantly at topographic irregularities. Similarly,

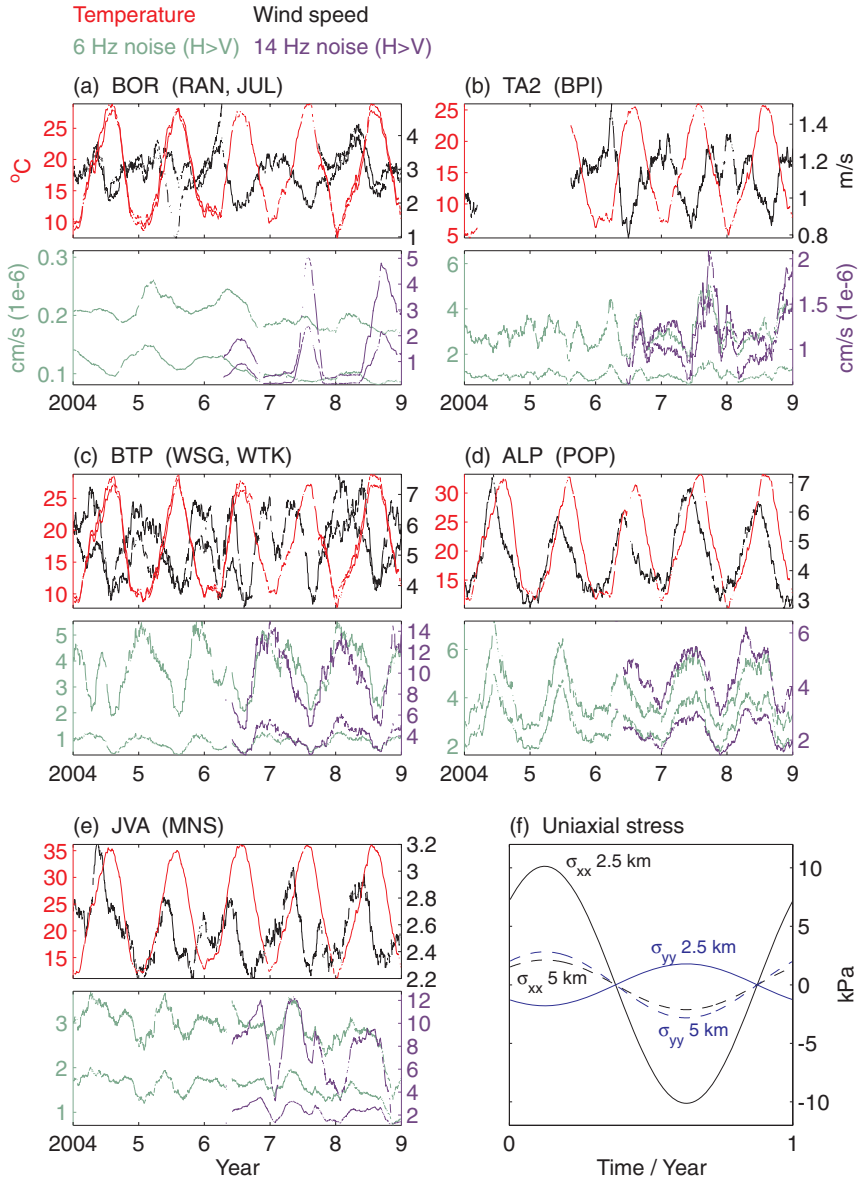

Figure 5. Comparison of meteorological (top figures) with seismic (bottom figures) data (a–e). Station codes in parenthesis correspond to CDEC meteorogical stations. Temperature (red) and wind speed (black) are measured within 20 km distance to each seismic station. We show seismic noise amplitudes for one frequency band below and above 10 Hz (colours as in Fig. 3). The horizontal amplitudes are consistently larger compared to the vertical (H > V). (a) Generation of noise at frequencies above 10 Hz is consistent with the thermoelastic strain hypothesis, since the noise time series correlates with temperature considering a phase shift. Wind speed is anticorrelated. Data from two weather stations are shown due to lack of data from the nearest station between 2006 and 2008. (b) Noise in 2007 and 2008 shows the same behaviour as in (a) with respect to temperature, yet some features show correlations with wind speeds. (c,d) Seismic noise likely dominated by local wind pattern. Note that temperature curves are inphase between c and d, whereas wind speeds are anticorrelated, despite the small distance between stations. (e) Signals at JVA are not consistently annually modulated, and hence do not correlate conclusively with one of the examined meteorological data. (f) Horizontal and vertical stress amplitudes computed at two depths using solutions from Berger (1975) with constants from Ben-Zion & Leary (1986), a shear modulus of 30 GPa and Poisson's ratio of 0.25.

thermoelastic strain generated near the surface by atmospheric temperature can lead to ongoing production of seismic noise. The observed high frequency noise may also reflect seismic radiation from continual occurrence of numerous local brittle failures below and around the stations, induced by sufficiently strong wind and thermoelastic strain. The low confining pressure at shallow depth (e.g. Sleep & Hagin 2008; Lyakhovsky *et al.* 2005) renders the subsurface material highly susceptible to recurring local failures. The integrated effect of seismic radiation generated (Mal & Knopoff 1967; Ben-Zion & Ampuero 2009) by ongoing displacement discontinuities and material damage in densely and broadly distributed source regions is expected to create a persistent flux of high frequency waves. In particular, thermoelastic strain may propagate with appreciable amplitude (and phase delay from atmospheric temperature of order 1–3 month) to mid crustal depth. Since this has not been discussed so far in the context of noise studies, we provide additional details below.

Berger (1975) obtained a solution for thermoelastic strain generated in elastic half-space by a travelling atmospheric thermal wave. Ben-Zion & Leary (1986) modified the solution to account

for a thin unconsolidated surface layer over the elastic solid and a stationary thermal source with length-scale related to topography and lateral material heterogeneities in a given area. When the surface temperature variations reach the boundary between the unconsolidated layer and underlying half-space, the induced thermoelastic strain propagates with appreciable amplitude to a depth of similar length scale as that of the surface temperature field. Ben-Zion & Leary (1986) showed that model-predicted thermoelastic strain from observed time series of atmospheric temperature fit very well seasonal variations that dominate strain-metre data in a 10 m deep tunnel in the San Gabriel mountains (near station BTP of Fig. 1). The amplitude of the predicted thermoelastic strain was an order of magnitude larger than the effect of seasonal water level changes of more than 10 m in a nearby (Bouquet) reservoir. Prawirodirdjo *et al.* (2006) used the same model and observed atmospheric temperature data to fit large-amplitude seasonal variations in 3 clusters of GPS instruments in southern California (near station groups ALP-EDW2-LDR, BBR-NVA-BLA and SLR-DGR-DNR; Fig. 1).

The forgoing theoretical and observational results predict annual and possibly sub-annual thermoelastic strain with significant amplitudes near the edges of topographic features, boundaries between water and rock bodies, etc. Such loadings are expected to produce seasonally modulated ongoing local failures in the top few kilometres of the crust with spatial distribution of amplitudes consistent with the observations of high-frequency seismic noise shown in Fig. 4 (and Fig. S2). We emphasize that the thermoelastic strains and stresses extend well below the depth of the seasonal temperature changes. For example, using the thermal constants employed by Ben-Zion & Leary (1986), annual temperature change of 40 °C with a spatial wavelength of 30 km produces stresses of ∼10 kPa and ∼3 kPa at depths of 2.5 km and 5 km, respectively (Fig. 5f). We also note that it is easier for thermal stresses to induce small failures in tectonically active prestressed environments. The ongoing occurrence of such localized failures increases, in turn, the level of stress heterogeneities and hence the prestress in some areas. The feedback between prestress and the discussed failures makes shallow rocks more prone to exhibit nonlinear attenuation during regular seismic events.

The amplitudes of the seasonal variations do not correlate with distance from the coast and appear to be especially strong near boundaries of topographic features (Figs 4 and S2), which is compatible with the dependence on wind speed and temperature changes filtered through the thermoelastic strain process. Many stations are near the perimeter and within the sparsely populated Mojave desert, where meteorological stations are scarce, show significant seasonal variations. We note that stations situated south of 34° in similarly arid locations, and at comparable topographic gradients (e.g. BOR), show consistently lower noise amplitudes and amplitude changes, and we do not observe a systematic reduction in wind speeds compared to other areas. The spatial pattern of observed amplitudes implies that the discussed ambient noise is unlikely to be dominated by ocean waves, variations of ground water levels and surface water flow. This is also supported by the existence of clear signals in both horizontal and vertical components (Figs 3 and S1). Changes in earthquake activity may also produce seasonal variations of noise, but apparent variations of seismicity have been associated with changes in network sensitivity (Atef *et al.* 2009), which may result in part from seasonal noise as demonstrated by our analysis.

To conclude, our results on systematically changing noise amplitudes at frequencies up to 18 Hz extend substantially the frequency range affected by seasonal variations. The high frequency noise is likely produced by a combination of wind speed induced elastic waves and ongoing widespread occurrence of shallow brittle failures caused by thermoelastic strain. A similar mechanism may explain seasonal variations of seismic velocities in the southern California area (Meier *et al.* 2010). A more complete analysis would examine additional variations of high frequency noise (e.g. some of the signals noted in Section 4), preferably in a borehole environment to separate depth dependent wind speed and temperature induced noise amplitudes. This will be the subject of future work.

ACKNOWLEDGMENTS

The seismograms used in this study were obtained from the Southern California Earthquake Data Center (SCEDC). We thank the scientists involved with recording and making the data available. GH thanks the computing staff at Caltech Seismolab for their continuous assistance. GH was supported in part by the Gordon and Betty Moore Foundation and by a postdoctoral fellowship with Jean-Paul Ampuero at Caltech. This is Caltech Tectonic Observatory Contribution 134. YBZ acknowledges support from the National Science Foundation (grant 354 EAR-0908903) and the Southern California Earthquake Center. The manuscript benefited from constructive comments of Norm Sleep, Keith Koper, an anonymous referee and Editor Cindy Ebinger. Some figures were made using GMT (Wessel & Smith 1998).

REFERENCES

Atef, A.H., Liu, K.H. & Gao, S.S., 2009. Apparent weekly and daily earthquake periodicities in the western United States, *Bull. seism. Soc. Am.*, **99**(4), 2273–2279, doi:10.1785/0120080217.

Beauduin, R., Lognonné, Montagner, J.P., Cacho, S., Karczewski, J.F. & Morand, M., 1996. The effects of the atmospheric pressure changes on seismic signals or how to improve the quality of a station, *Bull. seism. Soc. Am.*, **86**(6), 1760–1769.

Ben-Zion, Y. & Ampuero, J.-P., 2009. Seismic radiation from regions sustaining material damage, *Geophys. J. Int.*, **178**, 1351–1356, doi:10.1111/j.1365-246X.2009.04285.x.

Ben-Zion, Y. & Leary, P., 1986. Thermoelastic strain in a half space covered by unconsolidated material, *Bull. seism. Soc. Am.*, **76**(5), 1447–1460.

Berger, J., 1975. A note on thermoelastic strains and tilts, *J. geophy. Res.*, **80**(2), 274–277.

Berger, J., Davis, P. & Ekström, G., 2004. Ambient Earth noise: a survey of the Global Seismographic Network, *J. geophys. Res.*, **109**, B11307, doi:10.1029/2004JB003408.

Brudzinski, M.R. & Allen, R.M., 2007. Segmentation in episodic tremor and slip along Cascadia, *Geology*, **35**(10), 907–910, doi:10.1130/G23740A.1.

Fischer, A.D., Peng, Z. & Sammis, C.G., 2008a. Dynamic triggering of high-frequency bursts by strong motions during the 2004 Parkfield earthquake sequence, *Geophys. Res. Lett.*, **35**, L12305, doi:10.1029/2008GL033905.

Fischer, A.D., Sammis, C.G., Chen, Y. & Teng, T., 2008b. Dynamic triggering by strong-motion P and S waves: evidence from the 1999 Chi-Chi, Taiwan, Earthquake, *Bull. seism. Soc. Am.*, **98**(2), 580–592.

Gurrola, H., Minster, J.B., Given, H., Vernon, F., Berger, J. & Aster, R., 1990. Analysis of high-frequency seismic noise in the western United States and eastern Kazakhstan, *Bull. seism. Soc. Am.*, **80**(4), 951–970.

Kedar, S., Longuet-Higgins, M., Webb, F., Graham, N., Clayton, R. & Jones, C., 2008. The origin of deep ocean microseisms in the North Atlantic Ocean, *Proc. R. Soc. A*, **464**, 777–793, doi:10.1098/rspa.2007.0277.

Koper, K.D. & de Foy, B., 2008. Seasonal anisotropy in short-period seismic noise recorded in South Asia, *Bull. seism. Soc. Am.*, **98**(6), 3033–3045, doi:10.1785/0120080082.

Koper, K.D., de Foy, B. & Benz, H., 2009. Composition and variation of noise recorded at the Yellowknife Seismic Array, 1991-2007, *J. geophys. Res.*, **114**, B10310, doi:10.1029/2009JB006307.

Kurrle, D. & Widmer-Schnidrig, R., 2008. The horizontal hum of the Earth: a global background of spheroidal and toroidal modes, *Geophys. Res. Lett.*, **35**, L06304, doi:10.1029/2007GL033125.

Longuet-Higgins, M.S., 1950. A theory of the origin of microseisms, *Phil. Trans. R. Soc. London, Ser. A*, **243**, 1–35.

Lyakhovsky, V., Ben-Zion, Y. & Agnon, A., 2005. A viscoelastic damage rheology and rate- and state-dependent friction, *Geophys. J. Int.*, **161**, 179–190, doi:10.1111/j.1365-246X.2005.02583.x.

Mal, A.K. & Knopoff, L., 1967. Elastic wave velocities in two component systems, *IMA J. Appl. Math*, **3**(4), 376–387.

McNamara, D.E. & Buland, R.P., 2004. Ambient noise levels in the continental United States, *Bull. seism. Soc. Am.*, **94**(4), 1517–1527.

Meier, U., Shapiro, N.M. & Brenguier, F., 2010. Detecting seasonal variations in seismic velocities within Los Angeles basin from correlations of ambient seismic noise, *Geophys. J. Int.*, **181**, 985–996, doi:10.1111/j.1365-246X.2010.04550.x.

Nadeau, R.M. & Guilhem, A., 2009. Nonvolcanic tremor evolution and the San Simeon and Parkfield, California, earthquakes, *Science*, **325**, 191–193, doi:10.1126/science.1174155.

Peterson, J., 1993. *Observations and Modeling of Seismic Background Noise*, Open file rep., U.S. Geol. Surv.

Prawirodirdjo, L., Ben-Zion, Y. & Bock, Y., 2006. Observation and modeling of thermoelastic strain in SCIGN daily position time series, *J. geophys. Res.*, **111**, B02408, doi:10.1029/2005JB003716.

Rhie, J. & Romanowicz, B., 2004. Excitation of Earth's continuous free oscillations by atmosphere-ocean-seafloor coupling, *Nature*, **431**, 552–556.

Ringdal, F. & Bungum, H., 1977. Noise level variation at NORSAR and its effect on detectability, *Bull. seism. Soc. Am.*, **67**(2), 479–492.

Shapiro, N.M., Ritzwoller, M.H. & Bensen, G.D., 2006. Source location of the 26 sec microseism from cross-correlation of ambient seismic noise, *Geophys. Res. Lett.*, **33**, L18310, doi:10.1029/2006GL027010.

Sleep, N.H. & Hagin, P., 2008. Nonlinear attenuation and rock damage during strong seismic ground motions, *Geochem. Geophys. Geosty.*, **9**(Q10015), doi:10.1029/2008GC002045.

Tanimoto, T., 2005. The oceanic excitation hypothesis for the continuous oscillations of the earth, *Geophys. J. Int.*, **160**, 276–288, doi:10.1111/j.1365-246X.2004.02484.x.

Tanimoto, T., Ishimaru, S. & Alvizuri, C., 2006. Seasonality of particle motion of microseisms, *Geophys. J. Int.*, **166**, 253–266, doi:10.1111/j.1365-246X.2006.02931.x.

Webb, S.C., 2007. The Earth's "hum" is driven by ocean waves over the continental shelves, *Nature*, **445**, 754–756, doi:10.1038/nature05536.

Wessel, P. & Smith, W.H.F., 1998. New, improved version of the Generic Mapping Tools released,, *EOS, Trans. Am. geophys. Un.*, **79**(47), 579.

Young, C.J., Chael, E.P., Zagar, D.A. & Carter, J.A., 1994. Variations in noise and signal levels in a pair of deep boreholes near Amarillo, Texas, *Bull. seism. Soc. Am.*, **84**(5), 1593–1607.

Zhan, Z., Ni, S., Helmberger, D.V. & Clayton, R.W., 2010. Retrieval of Moho-reflected shear wave arrivals from ambient seismic noise, *Geophys. J. Int.*, **182**(1), 408–420, doi:10.1111/j.1365-246X.2010.04625.x.

Zhang, J., Gerstoft, P. & Shearer, P.M., 2009. High-frequency P-wave seismic noise driven by ocean winds, *Geophys. Res. Lett.*, **36**, L09302, doi:10.1029/2009GL037761.

SUPPORTING INFORMATION

Additional Supporting Information may be found in the online version of this article:

Figure S1. Results of noise amplitude measurements at all 30 stations indicated in Fig. 1. The results are organised as in Fig. 3.
Figure S2. Spatial distribution of maximum annual variations of the H noise amplitude. Values are obtained by subtracting the minimum from the maximum smoothed amplitude values in each calendar year (Fig. S1). We excluded amplitude steps of uncertain origin that occurred at some stations (e.g. steps in 2004 and 2007 at BLA). Similar to the (median) amplitude levels (Fig. 4), the largest amplitude changes are consistently measured at stations near strong topographic gradients in or around the Mojave desert. Blue dots correspond to stations indicated in Figs 1 and 3.
Figure S3. Scaled amplitude response function of station ARV, channel BHE, 40 Hz sampling. Amplitudes associated with the frequency band at 18 Hz are underestimated due to the effect of the anti-alias filter. Results of the 16 Hz data (filtered 15–17 Hz) do not show consistently reduced amplitudes.

Please note: Wiley-Blackwell are not responsible for the content or functionality of any supporting materials supplied by the authors. Any queries (other than missing material) should be directed to the corresponding author for the article.